A Comparative Study of the Use of the Generalized Hold Function for HDDs

Keitaro Ohno, *Member, IEEE*, Mitsuo Hirata, *Member, IEEE*, and Roberto Horowitz, *Member, IEEE*

***Abstract*—This paper is concerned with the application of $\mathcal{H}_\infty$ control with the generalized hold function (GHF) to track-following control of hard disk drives (HDDs). In HDDs, the sampling frequency is limited primarily by the fact that a high sampling frequency tends to decrease the available data storage capacity of the devices, since the position error signal (PES) must be stored on the disk. Under such conditions, GHF provides a possible way to enhance servo performance without requiring more PES data. In this paper, we investigate its possibility, comparing the results with other conventional $\mathcal{H}_\infty$ control design results, including continuous/discrete-time and single/multirate control. Our results show that this controller has better performance due to the nature of the control input of the GHF.**

***Index Terms*—Generalized hold function (GHF), $\mathcal{H}_\infty$ control, hard disk drives (HDDs), multirate, positioning.**

I. Introduction

MANY algorithms have been proposed so far for head-positioning control of hard disk drives (HDDs) in order to meet the tracking requirements that are necessary to achieve their ever-increasing track density requirements. Utilization of the $\mathcal{H}_\infty$ control design method is one possible way of enhancing the performance and robustness of HDD servo systems. This is because it can explicitly specify closed-loop specifications and systematically treat the tradeoff between control performance and robust stability. An early attempt can be found in [1], which was based on a simple continuous-time mixed-sensitivity problem. Since then, much research has focused on the $\mathcal{H}_\infty$ control design framework. However, it basically assumes zero-order hold function (ZOH). In a continuous-time $\mathcal{H}_\infty$ design, there is no way besides discretizing the resulting continuous-time controller at the sampling frequency. The effect of the jump in the measurement cannot be considered in this way, which induces a small step response at every sampling time. In a discrete-time $\mathcal{H}_\infty$ design, although this effect can be dealt with, there is no way to handle the intersample behavior. Sampled-data $\mathcal{H}_\infty$ design [2] provides a possible way to handle both of these effects, and some researchers [3] have been trying to take advantage of this feature for HDDs. However, it still assumes ZOH. Thus, this raises the issue of whether we can obtain better performance by introducing other types of hold functions.

In industry, the so-called multirate technique has been successfully developed and widely used. The basic idea is to introduce faster ZOH than sampling frequency. By using a higher control input update frequency, we can get wider control bandwidth. Multirate control itself was developed in the late 1950s, and an early application attempt to HDDs can be found in [4]. It proposed a way to design a multirate state estimator that is driven several times faster than the measurement sampling rate and yields open-loop estimation of intersample state so that the resulting control input becomes smoother. Hara and Tomizuka [5] extended their idea in order to achieve better estimation. Furthermore, recently, much effort has concentrated on the development of multirate control techniques based on the $\mathcal{H}_\infty$ control design framework, which include the discrete-time lifting technique-based [6] multirate $\mathcal{H}_\infty$ control [9], the zero-interpolator-based multirate $\mathcal{H}_\infty$ control [10], sampled-data multirate $\mathcal{H}_\infty$ control [7] for the dual-stage actuated HDDs [8], and frequency dividing technique-based multirate $\mathcal{H}_\infty$ control [11]. However, all the above design methods still assumed a ZOH as the hold function.

In this paper, we investigate the possibility of obtaining better performance by introducing a generalized hold function (GHF) in $\mathcal{H}_\infty$ control proposed by [12], which never assumes a ZOH. The basic idea of GHF is to generate control through a hold function that is optimized based on the dynamics of the controlled plant, while the output is sampled periodically. Thus, the GHF can yield continuous-time control input which jumps at the measurement sampling instant. This controller is derived so as to satisfy a given $\mathcal{H}_\infty$ performance requirement, which is defined in terms of the continuous-time domain. Thus, intersample behavior can be taken into consideration in a similar manner as in the sampled-data $\mathcal{H}_\infty$ control problem.

We first elaborate on how to obtain the controller. Then, a design example will be demonstrated in such a way that we can compare our results with those obtained by several other methods, including the continuous/discrete-time single/multirate $\mathcal{H}_\infty$ controllers.

II. $\mathcal{H}_\infty$ Controller With Generalized Hold Function

In this paper, we consider the linear system of the form

$$\mathcal{G}: \begin{cases} \dot{x}(t) = Ax(t) + Bw(t) + Eu(t) \\ z(t) = Cx(t) + Du(t) \\ y(ih) = Hx(ih) + v(ih) \end{cases} \tag{1}$$

Manuscript received January 3, 2003; revised January 27, 2004.

K. Ohno is with the Autonomous System Laboratory, Fujitsu Laboratories, Ltd., Kanagawa 243-0197, Japan (e-mail: keitaro.ohno@nifty.com).

M. Hirata is with the Department of Electrical and Electronic Engineering, Utsunomiya University, Tochigi 321-1717, Japan (e-mail: hirata@cc.utsunomiya-u.ac.jp).

R. Horowitz is with Department of Mechanical Engineering, University of California, Berkeley, CA 94720-1740 USA (e-mail: horowitz@me.berkeley.edu).

Digital Object Identifier 10.1109/TMECH.2004.842244

where $x \in \mathbb{R}^n$ is the state of the system, $y \in \mathbb{R}^p$ is the sampled discrete-time measurement, $u \in \mathbb{R}^r$ is the control input, $w \in \mathbb{R}^m$ is the external disturbance, $v \in \mathbb{R}^p$ is the discrete-time measurement noise, h is the sampling time, and i is the natural number. Also, the following standard assumptions are made.

A1) The discrete-time system $(e^{Ah}, \tilde{B}, H)$ is stabilizable and detectable.

A2) The continuous-time system (A, E, C) is stabilizable and detectable.

A3) $D'[C \quad D] = [0 \quad I]$

where $\tilde{B}$ is defined as follows:

$$\tilde{B} := \left(\int_0^h e^{At} BB' e^{A't} dt \right)^{1/2}. \tag{2}$$

The controller that we are dealing with can be obtained based on the results of [12], as follows.

Theorem 1 ([12]): Consider the system described by (1). Let $\gamma > 0$ be given. Suppose that assumptions A1)–A3) hold. Define the following performance measure:

$$J_0(\mathcal{K}) := \sup \left\{ \left[\frac{\|z\|^2}{\|w\|^2 + \|v\|^2} \right]^{1/2} \right\}. \tag{3}$$

Then there exists an internally stabilizing controller such that $J_0(\mathcal{K}) < \gamma$ if, and only if, the following conditions hold.

1) There exists a unique real symmetric matrix P which satisfies the following continuous-time Riccati equation:

$$A'P + PA + C'C + P(\gamma^{-2}BB' - EE')P = 0 \tag{4}$$

such that $A + (\gamma^{-2}BB' - EE')P$ has all the eigenvalues inside the open left-half plane, and $P \geq 0$.

2) Define

$$\begin{aligned} \Pi(t) &:= \begin{pmatrix} \Pi_{11}(t) & \Pi_{12}(t) \\ \Pi_{21}(t) & \Pi_{22}(t) \end{pmatrix} \\ &= \exp\left\{ \begin{pmatrix} (A + \gamma^{-2}BB'P)' & \gamma^{-2}PEE'P \\ -BB' & -(A + \gamma^{-2}BB'P) \end{pmatrix} t \right\}. \end{aligned} \tag{5}$$

There exists a real symmetric matrix $Q \geq 0$ satisfying

$$\Pi_{21}(h) + \Pi_{22}(h)Q = Q(I + H'HQ)^{-1}(\Pi_{11}(h) + \Pi_{12}(h)Q) \tag{6}$$

such that $(I + H'HQ)^{-1}(\Pi_{11}(h) + \Pi_{12}(h)Q)$ has all its eigenvalues inside the open unit disk, and $\Pi_{11}(t) + \Pi_{12}(t)Q$ is nonsingular for all $t \in [0, h]$. Moreover, if such P, Q exist, then the corresponding controller $\mathcal{K}_{PQ}$ of the form

$$\begin{aligned} \hat{x}(ih) &= (I + QH'H)^{-1} \\ &\quad \cdot \left(e^{(A+\gamma^{-2}BB'P - EE'P)h} \hat{x}((i-1)h) + QH'y(ih) \right) \\ \hat{x}(0) &= 0 \\ u(t) &= -E'Pe^{(A+\gamma^{-2}BB'P - EE'P)(t-ih)} \hat{x}(ih) \\ &\quad t \in [ih, (i+1)h) \end{aligned} \tag{7}$$

is an internally stabilizing controller and achieves $J_0(\mathcal{K}_{PQ}) < \gamma$.

■

The above theorem states that solving two Riccati equations via the γ iteration yields a $\mathcal{H}_\infty$ controller with a GHF. The continuous-time Riccati equation (4) is of a standard form, while the discrete-time Riccati equation (6) is not. However, as [12] pointed out, it is easy to solve this equation by thinking of the following equivalent form

$$\Pi(h) \begin{bmatrix} I \\ Q \end{bmatrix} = L \begin{bmatrix} I \\ Q \end{bmatrix} S_Q \tag{8}$$

where

$$\begin{aligned} L &:= \begin{bmatrix} I & H'H \\ 0 & I \end{bmatrix} \\ S_Q &:= (I + H'HQ)^{-1}(\Pi_{11}(h) + \Pi_{12}(h)Q) \end{aligned} \tag{9}$$

and S_Q has all its eigenvalues inside the open unit disk. Notice that (8) can be translated to a standard eigenvalue problem of $L^{-1}\Pi(h)$ on the ground that L is always nonsingular.

Using the aforementioned techniques, we can calculate the controller. However, this form has a complexity when making a direct comparison with other controllers in terms of frequency characteristics, since the $\mathcal{H}_\infty$ generalized hold controller is a hybrid system of continuous-time and discrete-time signals. Here, for convenience, a method of calculating the open-loop frequency characteristics is proposed by showing a transfer function of discrete-time equivalent of open-loop system for GHF. First, re-define the controller in (7)

$$\begin{aligned} \hat{x}(ih) &= A_c \hat{x}((i-1)h) + B_c y(ih) \\ u(t) &= C_c e^{D_c(t-ih)} \hat{x}(ih) \end{aligned} \tag{10}$$

where

$$\begin{aligned} A_c &:= (I + QH'H)^{-1} e^{(A+\gamma^{-2}BB'P - EE'P)h} \\ B_c &:= (I + QH'H)^{-1} QH' \\ C_c &:= -E'P \\ D_c &:= (A + \gamma^{-2}BB'P - EE'P). \end{aligned} \tag{11}$$

Then, the nominal controlled plant can be written as follows:

$$\begin{aligned} \dot{x}(t) &= Ax(t) + Eu(t) \\ y(t) &= Hx(t). \end{aligned} \tag{12}$$

Moreover, $u(t)$ in (10) can be represented as a solution to the following differential equation:

$$\begin{aligned} \dot{x}_k(t) &= D_c x_k(t) \\ u(t) &= C_c x_k(t) \\ &\quad t \in [ih, (i+1)h),\ x_k(ih) = \hat{x}(ih). \end{aligned} \tag{13}$$

From (12) and (13), we have the following augmented system for $t \in [ih, (i+1)h]$, $x_k(ih) = \hat{x}(ih)$:

$$\begin{bmatrix} \dot{x}(t) \\ \dot{x}_k(t) \end{bmatrix} = \begin{bmatrix} A & EC_c \\ 0 & D_c \end{bmatrix} \begin{bmatrix} x(t) \\ x_k(t) \end{bmatrix}. \tag{14}$$

By taking an integral of (14) for $t \in [ih, (i+1)h]$, we have

$$\begin{aligned} x((i+1)h) &= [I \quad 0] \exp\left(\begin{bmatrix} A & EC_c \\ 0 & D_c \end{bmatrix} h \right) \begin{bmatrix} x(ih) \\ \hat{x}(ih) \end{bmatrix} \\ &= [e^{Ah} \quad M] \begin{bmatrix} x(ih) \\ \hat{x}(ih) \end{bmatrix} \\ M &:= [I \quad 0] \exp\left(\begin{bmatrix} A & EC_c \\ 0 & D_c \end{bmatrix} h \right) \begin{bmatrix} 0 \\ I \end{bmatrix}. \end{aligned} \tag{15}$$

It follows that

$$\begin{aligned} x((i+1)h) &= e^{Ah} x(ih) + M\hat{x}(ih) \\ &= e^{Ah} x(ih) + M\left(A_c x((i-1)h) + B_c y(ih)\right). \end{aligned} \tag{16}$$

By augmenting the system of (16) along with (10), we have the following discrete equivalent of open-loop system:

$$\mathcal{PK}_{\mathcal{PQ}} = \left[\begin{array}{cc|c} e^{Ah} & MA_c & MB_c \\ 0 & A_c & B_c \\ \hline H & 0 & 0 \end{array} \right] \tag{17}$$

where $\mathcal{P}$ is a controlled plant.

III. Design of Track-Following Controllers With a Generalized Hold Function

In this section, a practical design methodology for track-following controllers with GHF for HDDs is discussed.

Let us first review assumptions A1)–A3) that were initially introduced by [12] for simplicity. These assumptions actually impose some restrictions on the construction of generalized plant. For example, so-called mixed-sensitivity problem with frequency-dependent weighting functions violates the assumption A3). As [12] pointed out, these assumptions can be relaxed to a general case in the same manner as the standard $\mathcal{H}_\infty$ control problem. However, generalization of theory is not our purpose. Hence, we consider the generalized plant and weighting functions which achieve a satisfactory good performance from the practical point of view within these assumptions. One way to satisfy these conditions for our purpose, which is the control design of single-input and single-output system HDDs, can be obtained by using the generalized plant shown in Fig. 1.

In this figure, α, β, and η are all strictly positive real scalar, and $\mathcal{W}$ is a frequency weighting function to the sensitivity function, which should be selected as a strictly proper stable transfer function to satisfy assumptions A1) and A3).

Regarding the controlled plant $\mathcal{P}$, first we have identified the plant model by using about ten, 33k-TPI, 7200 rpm commercial drives, of which the sampling frequency is 10 kHz. The identified model is shown in Fig. 2 as a thin solid line labeled as the "Actual Model." Regarding mechanical resonance modes, from the assumption A1)-A3), it is difficult to treat the robust problem for them appropriately in $\mathcal{H}_\infty$ framework. Thus, two resonance modes at a frequency of 5.2 and 6.2 kHz, which are usually called butterfly modes, are respectively compensated for by a second-order notch filter, whose parameters are the same as those used in commercial drives. This notch-compensated model is also shown in the same figure as a dotted line

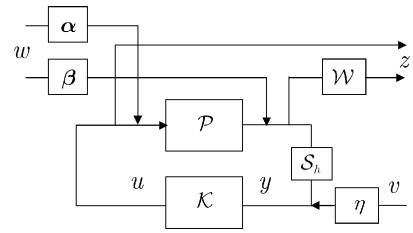

Fig. 1. Construction of generalized plant that satisfies the conditions A1)–A3). α, β, and η are all scalar constant, $\mathcal{W}$ is a frequency weighting function, and $\mathcal{S}$ is a sampler. Note that y is a discrete-time signal while u is a continuous-time signal.

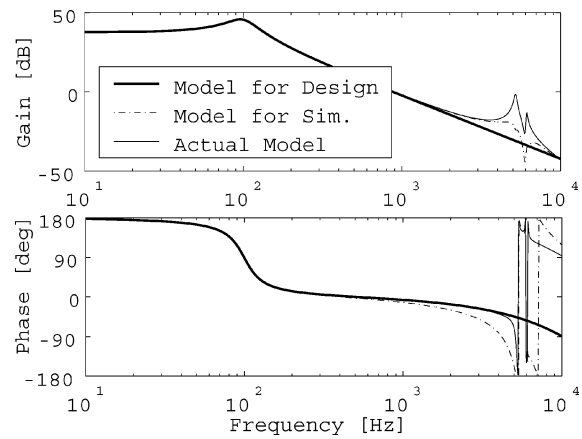

Fig. 2. Frequency response of plant model for design. Model for simulation (Model for Sim.) are also shown along with its real model (Actual Mode). A couple of resonant modes at the frequency range of 5–8 kHz, which is expected to be perturbed by 5%–10% caused by unit-by-unit variation or temperature fluctuation, are usually compensated for by a series of several notch filters successfully.

labeled "Model for Sim." Literally, this model will be used for simulation. For design purposes, we use the following fourth-order model with some time-delay that is realized by the Padé approximation

$$\mathcal{P} = \frac{-3 \times 10^7}{s^2 + 251.3s + 3.948 \times 10^5} \cdot \frac{s^2 - 2.4 \times 10^5 s + 1.92 \times 10^{10}}{s^2 + 2.4 \times 10^5 s + 1.92 \times 10^{10}}. \tag{18}$$

The first term on the right-hand side of this equation stands for a resonant mode at 100 Hz with damping factor of 0.2, which is usually called the rigid body mode. The last term stands for the Padé approximation for a time delay of 25 μs. The frequency response of this model is also depicted in the same figure.

Regarding the frequency weighting function $\mathcal{W}$ for shaping the sensitivity function, we have selected the following second-order filter after several trial-and-errors

$$\mathcal{W} = \frac{9.219 \times 10^{-4} s + 1}{6.959 \times 10^{-3} s + 1} \cdot \frac{0.1737}{3.979 \times 10^{-5} s + 1} \kappa \tag{19}$$

where κ is a scalar constant which will be described later. The first term on the right-hand side of (19) is that of a phase-lag filter with a center frequency of 62.8 Hz and a phase-lag of 50°, and it is introduced to attenuate low-frequency disturbances, which are primarily caused by air flow through disk rotation. The second term in (19) is that of a low-pass filter, whose cutoff frequency is 4 kHz, and is introduced so that the transfer

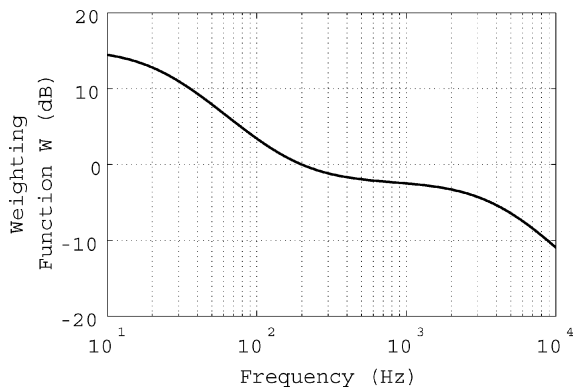

Fig. 3. Frequency response of weighting function $\mathcal{W}$. Note that the actual specification of sensitivity function is $\beta\mathcal{W}$.

function is strictly proper and the peak gain of the resulting sensitivity function is specified. Moreover, $\mathcal{W}$ is scaled so that the open-loop system's gain crossover frequency is around 1 kHz. The frequency response of $\mathcal{W}$ is depicted in Fig. 3. Notice that the actual specification of the sensitivity function becomes $\beta\mathcal{W}$, as can be seen from Fig. 1.

Regarding the scalar constant that represents the magnitude of measurement noise η in Fig. 1, [12] assumed that $\eta = 1$. However, by multiplying the output equation in (1) by $1/\eta$, this problem with $\eta \neq 1$ easily comes down to that with $\eta = 1$.We have selected $\eta = 0.01$ for a practical design. Regarding the other two constants α and β, they were, respectively, set to 0.333 and 0.173, after several trial-and-errors.

Using the above generalized plant, a controller with γ of 0.995 was obtained. The following are the two solutions to the Riccati equations P and Q, shown at the bottom of the page.

Now, we can compute every parameter in (7). Let us take a look again at the controller with GHF. The controller contains a linear time-invariant discrete-time system with state variable $\hat{x}$, and a linear time-varying continuous-time feedback gain, which is nothing but the representation of GHF and is of most interest. This time-varying feedback gain, which is often referred to as an output distribution matrix of the controller, or simply the C matrix, is a periodic function of time for every sampling period, as shown in Fig. 4.

Since the output of controller is a product of this time-varying vector and a constant state variable, it becomes a continuous function during the intersample period. It should be pointed out that, although the time-varying vector looks quite smooth in our design case, it does not necessarily mean that it cannot yield oscillatory behavior of control input since the term in the exponential in (7) may have complex eigenvalues.

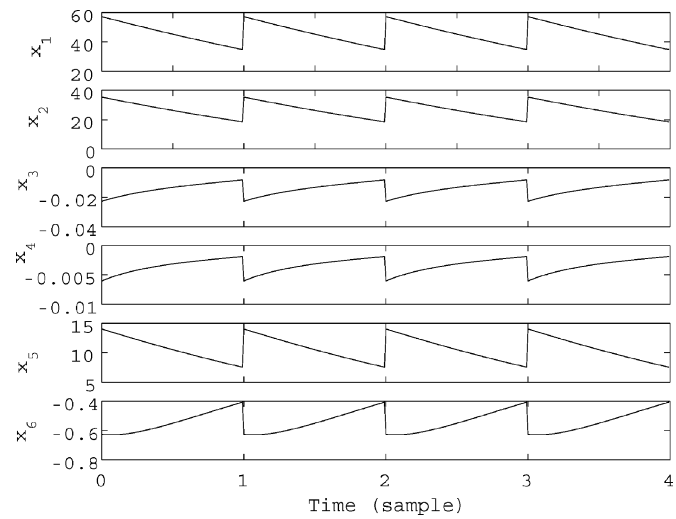

Fig. 4. Intersample behavior of each element of time-varying feedback gain. Corresponding states to the first four variables come from the plant model and the last two come from the frequency weighting function.

By taking advantage of this nature of the GHF, we can use a wider frequency range for the control input. This can be translated as a recovery of phase, and it leads to a reduction in the peak gain of the sensitivity function. In other words, it constitutes an additional design degree of freedom which improves performance, in the similar manner as does the multirate design framework. Notice that intersample continuity of the control input does not at all imply the continuity over consecutive sampling periods since we have jumps of measurements at every sampling period.

We will evaluate the performance of this controller and compare it with controllers designed by other methods.

IV. Comparative Study on the Tracking Performance

In this section, the tracking performance of the $\mathcal{H}_\infty$ controller with GHF that was designed in the previous section is evaluated by comparing it with the other design methods. The following six cases are considered:

$$P \times 10^3 = \begin{bmatrix} +860.408 & +643.967 & -1.698\,27 & -0.481\,55 & +259.883 & +24.9617 \\ +643.967 & +508.863 & -1.603\,70 & -0.455\,10 & +206.153 & +27.2183 \\ -1.698\,27 & -1.603\,70 & +0.062\,80 & +0.011\,49 & -1.108\,35 & -2.100\,62 \\ -0.481\,55 & -0.455\,10 & +0.011\,49 & +0.003\,76 & -0.238\,86 & -0.240\,37 \\ +259.883 & +206.153 & -1.108\,35 & -0.238\,86 & +88.6975 & +32.1232 \\ +24.9617 & +27.2180 & -2.100\,62 & -0.240\,37 & +32.1232 & +96.8404 \end{bmatrix}$$

$$Q \times 10^3 = \begin{bmatrix} +1672.93 & -1543.07 & -17.2817 & +4.020\,07 & +90.4502 & +23.8766 \\ -1543.07 & +1426.61 & +17.3010 & -3.951\,18 & -82.5538 & -21.1866 \\ -17.2817 & +17.3010 & +1.906\,87 & -0.001\,85 & -0.631\,31 & -0.000\,63 \\ +4.020\,07 & -3.951\,18 & -0.001\,85 & +0.175\,10 & +0.156\,82 & +0.000\,33 \\ +90.4502 & -82.5538 & -0.631\,31 & +0.156\,82 & +667.729 & -16.5355 \\ +23.8766 & -21.1866 & -0.000\,63 & +0.000\,33 & -16.5355 & +42.4607 \end{bmatrix}.$$

C1) continuous-time $\mathcal{H}_\infty$ controller;
C2) discretized continuous-time $\mathcal{H}_\infty$ controller without considering the time delay caused by ZOH effect;
C3) discretized continuous-time $\mathcal{H}_\infty$ controller with considering the corresponding time delay caused by ZOH effect;
C4) discrete-time $\mathcal{H}_\infty$ controller;
C5) $3 \times$ Multirate $\mathcal{H}_\infty$ controller designed by the discrete-time lifting technique and discrete-time $\mathcal{H}_\infty$ control method;
C6) $\mathcal{H}_\infty$ controller with the GHF proposed in this paper.

C1) will be considered to be the "ideal case" where a continuous-time position error signal (PES) measurement is assumed to be available. Thus, its corresponding tracking performance can be thought of as a best achievable performance. Three cases from C2) to C4) are all single-rate design examples, and C5) and C6) utilize the intersample control input to improve performance. In all of the above cases, an accurate enough simulator, which will be described later in detail, is used to evaluate tracking performance. In cases C4) and C5), the weighting function $\mathcal{W}$ in (19) is discretized by the standard bilinear transformation while plant model $\mathcal{P}$ is discretized by ZOH method. In the multirate design case of C5), intersample behavior of control input is evaluated ten times weaker than that at measurement sampling instants. Note that in each design procedure, no parameter tune up is made, except for κ, in order to compare the results evenly. This also means that all the design settings, including weighting functions made in the previous section, are not the best for all the cases. The choice of κ for each design will be described later.

To evaluate tracking performance, we use an accurate enough simulator, which was developed on a commercial software for control system design, and it has been correlated to the response of actual drives so that it has an accuracy within 1% in terms of average track misregistration (TMR), or tracking error, for about ten drives when the precise disturbance model of an actual HDD is used. A similar detailed HDD model can be found in [13].

In this simulator, two kinds of disturbance model are considered

D1) white disturbance to be added to the control input;
D2) precise disturbance models in actual HDDs, to be added at appropriate points.

Case D1) is considered in order to compare the performance of controllers impartially. The realistic disturbances in D2) sometimes make it difficult to compare the results because these disturbances tend to contain much more complicated color. The white disturbance in D1) corresponds to what is referred to in the industry as windage disturbance. This disturbance is caused by internal air flow induced by disk rotation, and its spectrum is almost white in acceleration order. On the other hand, case D2) is used to evaluate the overall performance of a drive when realistic disturbances are injected. This disturbance model is actually estimated from the average of about ten drives by measuring the PES. Then, by subtracting the sensitivity function of what is used when PES is measured, and also by considering the ZOH effect, the precise disturbance model is estimated. Notice that these disturbances vary among different manufacturers and drive models. Fig. 5 shows the estimated disturbance model. After obtaining this model, it is divided into several components that are basically categorized by its cause, e.g., windage, disk flutter, decode noise, etc. Each component is injected to the corresponding appropriate point in the simulator in order to have an accurate estimation of the TMR.

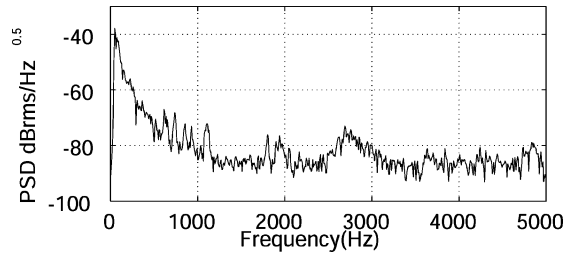

Fig. 5. Estimated disturbance model, which will be called D2) disturbance in this paper. This model is obtained from the average of several tens of drives.

TABLE I
SUMMARY OF DESIGN RESULTS WHEN $\kappa = 1$ BASIS

$\mathcal{K}$	D1)TMR	D2)TMR	γ	Bw(Hz)	Gm(dB)	Pm(deg)
C1)	0.1347	0.0603	0.673	754	10.1	36.6
C2)	0.1622	0.0764	0.763	768	5.2	23.0
C3)	0.1615	0.0690	N/A	718	6.7	31.6
C4)	0.1651	0.0701	0.773	704	6.8	31.1
C5)	0.1801	0.0793	0.214	684	6.3	27.1
C6)	0.1257	0.0624	0.994	830	6.2	36.6

Moreover, the sensitivity function of the closed-loop system is estimated in this simulator by using the following technique. First, we add some band-limited white noise at the control input, then we store the time-domain signals of the added noise itself and the sum of the noise and control input. Then, by taking the cross spectrum of these two signals over the power spectrum of the noise signal, we can estimate the sensitivity function [14]. Notice that, in this paper, all the open-loop gain crossover frequencies, gain margins, and phase margins are estimated using this method.

A. TMR and Frequency-Domain Analysis When $\kappa = 1$

TMR and frequency characteristics are analyzed here for the case when κ defined in (19) is set to $\kappa = 1$. This implies that the same weighting function including a couple of scalar constants is used for all the control cases except for C5) as we have mentioned at the beginning of this section. The results are summarized in Table I. In this table, each column has the following meaning. $\mathcal{K}$: Controller. D1)TMR: 6σ rms standard deviation of the PES for the analysis case D1). D2)TMR: 6σ rms standard deviation of PES for the analysis case D2). Bw: Open-loop gain crossover frequency. Gm: Gain margin. Pm: Phase margin. Note that κ for case C3) is not applicable since this controller is obtained by just discretizing the controller in case C2).

First, it is easy to see from the results of C2)-C3) that the simple continuous-time design without considering any effect of ZOH does not meet our requirement since the phase margin is too small; however, if we consider the corresponding time delay by using the Padé approximation, the result becomes quite similar to that of discrete-time design. Thus, from here on, we will not consider the C2)–C3) cases.

TABLE II
SUMMARY OF DESIGN RESULT ON THE BASIS OF $\gamma = 1$ BASIS

$\mathcal{K}$	D1)TMR	D2)TMR	κ	Bw(Hz)	Gm(dB)	Pm(deg)
C1)	0.1084	0.0569	2.568	884	8.7	33.8
C2)	0.1415	0.0770	1.870	906	3.8	18.0
C3)	0.1418	0.0668	N/A	798	5.6	29.2
C4)	0.1472	0.0683	1.777	776	6.0	28.9
C5)	0.1287	0.0647	6.586	830	5.6	35.1
C6)	0.1257	0.0624	1.000	830	6.2	36.6

Second, the best TMR for both the D1) and D2) analysis cases is obtained by the GHF-driven $\mathcal{H}_\infty$ controller, i.e., C6), and its open-loop characteristics in terms of gain margin and phase margin are both within a satisfactory range.

Third, the achieved γ for C6) is a little bit higher than in other cases. This implies this method tends to yield rather conservative controller since it evaluates the intersample behavior in continuous-time signal sense. Notice that C5) has a little bit lower achieved γ. One may think of this as being a contradiction since C5) also can be thought to evaluate the intersample behavior approximately in a discrete-time signal sense. However, we have used a slightly different weighting in the generalized plant for multirate design case. Thus, it is difficult to make a direct comparison between C5) and the other cases in terms of γ.

Fourth, the achieved γ is different case by case, which implies that it is not evenly compared. Thus, in order to make a comparative study, we need to adjust the weighting so that every γ is at the same level, and we will discuss this procedure in the following subsection.

B. TMR and Frequency-Domain Analysis on the Basis of $\gamma = 1$

In order to gain further insight into the comparative performance of each controller, a simple modification to each weighting function was used so that each result can be comparable to each other. The strategy is as follows. Find the maximum κ that satisfies $\gamma \leq 1$ for each control design, where κ is the constant gain of $\mathcal{W}$, as described in (19). A standard bisection method was used to find the κ for each controller and the results are summarized in Table II.

Now, all results are comparable with each other since we have $\gamma = 1$ for all the cases. Except for the ideal case C1), the best positioning accuracy in terms of TMR is still obtained by C6) in both the cases of D1) and D2), and the percentage improvement of TMR when compared to the single-rate case C4) is around 10%. Furthermore, the controller C6) still has a performance advantage over the multirate controller C5). It can also be seen that Gm, Pm, and Bw in this table for both C5) and C6) are similar. In order to check the difference, open-loop frequency responses for all the cases but C2) and C3) are depicted in Fig. 6. Notice that, for controller C6), the technique described in (17) was used.

First, as we have seen in Table II, both C5) and C6) have a higher bandwidth and a higher phase recovery when compared to the single-rate design case of C4), which results in gaining lower sensitivity peak gain around the gain crossover frequency ($\simeq$ 800 Hz). This is why C5) and C6) have better performance than all single-rate design cases and is made possible by taking advantage of the intersample design degree of freedom with respect to the control input.

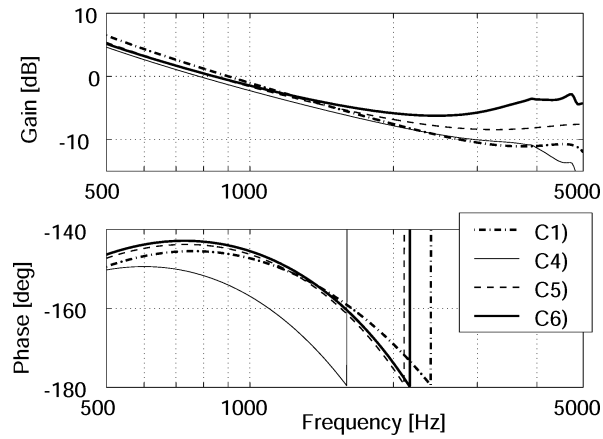

Fig. 6. Open-loop frequency responses. Frequency characteristics of C5) is similar to that of C6).

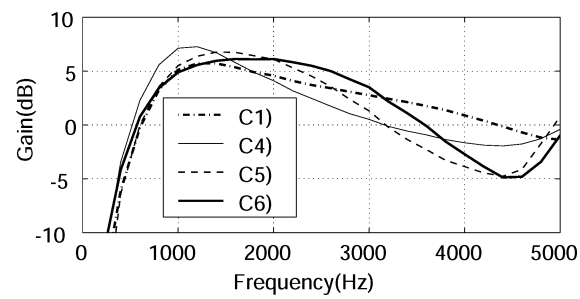

Fig. 7. Sensitivity function. C5) and C6) have similar features.

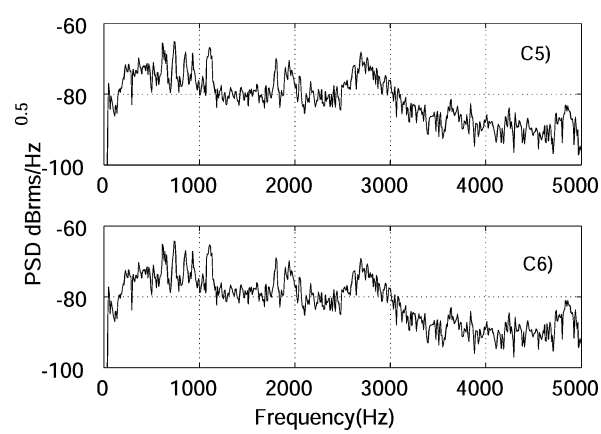

Fig. 8. Comparison of the power spectral density of the position error signal.

Second, we can see from Fig. 6 that C5) and C6) have quite similar open-loop frequency characteristics. In order to compare them further, their sensitivity functions are estimated as shown in Fig. 7, by using the technique described at the beginning of this section, which implies the best estimate of actual sensitivity function. The corresponding power spectrum of the PES for both of the C5) and C6) cases are depicted in Fig. 8. From these figures, we cannot yet observe distinctive difference. In the following subsection, we will compare these controllers in the time domain.

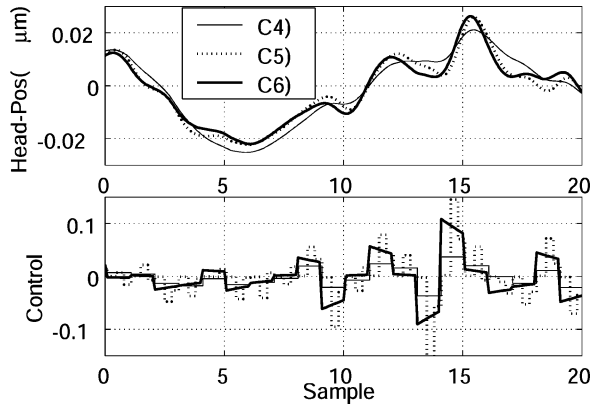

Fig. 9. Comparison of time-response of control input. Although the loop characteristics of C5) and C6) are similar, intersample behavior of control input are quite different.

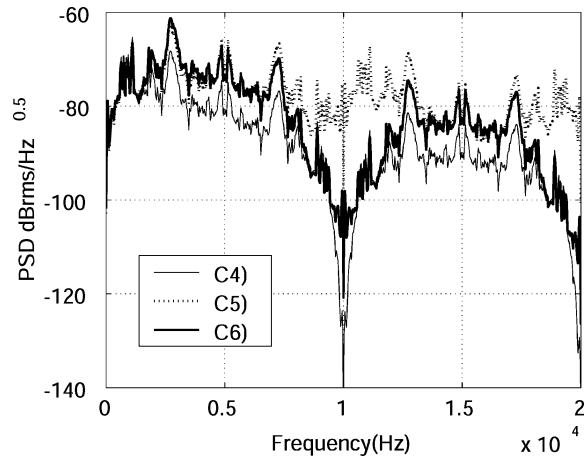

Fig. 10. Comparison of power spectral density of control input.

TABLE III
SUMMARY OF POWER CONSUMPTION (NONDIMENSIONAL UNIT)

Case	C1)	C2)	C3)	C4)	C5)	C6)
Power Consumption	0.838	1.01	0.90	0.85	1.72	1.51

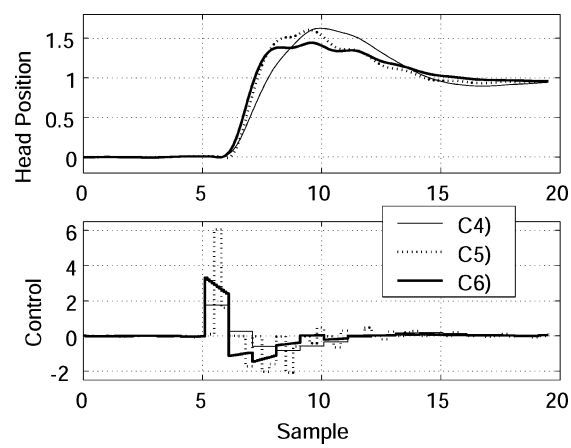

Fig. 11. Comparison of current and head position for step response.

C. Time-Domain Analysis

In Fig. 9, the time-response of the head position (upper) and control input (lower) during the track-following operation are depicted for different controllers C4)–C6), where the D2) disturbance model was used. Now, we can see that, although the open-loop characteristics of C5) and C6) are similar, the intersample behavior of their control input is quite different. Note that the behavior of head position remains similar, although there is a slight phase delay in C5) when compared to that in C6). This can be interpreted as the reason why we have not observed a distinctive difference in frequency-domain analysis. Interesting discussion regarding the intersample behavior of the GHF in comparison with ZOH can be found in [15].

The control input in C6) tends to rise abruptly at the measurement, and then tends to decrease exponentially during the sample period. On the other hand, the control input in C5) tends to rise slowly at the measurement, and then abruptly tries to compensate for the delay. Fig. 10 depicts the power spectrum of the control input during track-following for these cases. Now, the difference is clear. Up to the Nyquist frequency, there is no difference between C5) and C6). However, at the frequency region where the power usually drops because of the effect of ZOH as can be seen in the single-rate design in C4), the case C5) still keeps its power, while that of C6) has dropped more than that of C5). This is one way to understand why C5) requires more energy to obtain the same position accuracy as C6). Note that the power consumption can be reduced by 12% if we use C6) instead of C5), as we can see from the summary in Table III.

Next, let us look at the comparison of step response that is depicted in Fig. 11, where the head position (upper) and control input (upper) are shown. First, we can see that both C5) and C6) have a much faster response as compared to C4). However, C5) requires almost double the control input. In addition, the overshoot in C5) is almost the same as C4) while that of C6) is reduced by 10%.

D. Implementation on a DSP

We have demonstrated several advantages of using a $\mathcal{H}_\infty$ controller with GHF. This controller can actually be implemented as an analog circuit. However, an analog implementation is not so attractive from the cost effectiveness point of view. Thus, it is desirable to implement this controller on a DSP as a digital controller, and it is actually feasible by simply using some fast hold function so as to thin out the time-varying vector in Fig. 4. It should be pointed out that this scheme does not guarantee $J_o < \gamma$ unless the substituted hold function is a good enough representing of the GHF. Table IV shows the effect of using a fast ZOH, which has the same structure we usually use for standard multirate controller. Note that MRR stands for multirate ratio, and the case MRR $= \infty$ is the original GHF result.

We can see from this table that we can use fast ZOH without considerable performance deterioration, even for the case when MRR $= 2$, whose TMR result is still better than that for the case C5) with MRR $= 3$. This shows that this method can be thought of as a feasible way to implement the GHF on a DSP. Notice that these results are reasonably reliable since the structure of the controller is the same as the conventional multirate controller, on which we base the simulation accuracy.

TABLE IV
IMPLEMENTATION ON A DSP

$\mathcal{K}$	MRR	D2)TMR	Bw(Hz)	Gm(dB)	Pm(deg)
C6)	16	0.0625	830	5.7	36.5
C6)	8	0.0632	794	6.2	36.5
C6)	4	0.0635	792	6.2	36.3
C6)	2	0.0638	806	6.6	35.4
C6)	∞	0.0624	830	6.2	36.6
C5)	3	0.0647	830	5.6	35.1

V. CONCLUSION

We have investigated the possible performance enhancements for track-following control of HDDs that can be attained with a $\mathcal{H}_\infty$ controller with a GHF by conducting several precise simulations, and we have compared the results with other design results, including continuous/discrete-time single/multirate $\mathcal{H}_\infty$ control. Our results show that the proposed controller has better performance when compared to conventional $\mathcal{H}_\infty$-based controllers. We have also confirmed that the time-response of the control input is much different than the others, and less control input is required to maintain a level of performance that is comparable to the multirate design case. This leads to lower power consumption. We have also confirmed that, due to the nature of the control input, step response can be improved.

ACKNOWLEDGMENT

The authors would like to thank Prof. S. Hara of the University of Tokyo for introducing important information.

REFERENCES

[1] M. Hirata, K. Z. Liu, T. Mita, and T. Yamaguchi, "Head positioning control of a hard disk drive using $\mathcal{H}_\infty$ theory," in *Proc. 31st IEEE Conf. Decision and Control*, vol. 2, Dec. 1992, pp. 2460–2461.

[2] P. T. Kabamba and S. Hara, "Worst-case analysis and design of sampled-data control systems," *IEEE Trans. Autom. Control*, vol. 38, no. 9, pp. 1337–1357, Sep. 1993.

[3] M. Hirata, T. Atsumi, A. Murase, and K. Nonami, "Following control of a hard disk drive by using sampled-data $\mathcal{H}_\infty$ control," in *Proc. IEEE Int. Conf. Control Applications*, Aug. 1999, pp. 182–186.

[4] W.-W. Chiang, "Multirate state-space digital controller for sector servo systems," in *Proc. 29th IEEE Conf. Decision and Control*, Dec. 1990, pp. 1902–1907.

[5] T. Hara and M. Tomizuka, "Multi-rate controller for hard disc drive with redesign of state estimator," in *Proc. American Control Conf.*, 1998, pp. 898–903.

[6] T. Chen and B. Francis, *Optimal Sampled-Data Control Systems*. New York: Springer-Verlag, 1996.

[7] T. Chen and L. Qiu, "$\mathcal{H}_\infty$ design of general multirate sampled-data control systems," *Automatica*, vol. 30, no. 7, pp. 1139–1152, 1994.

[8] J. Ishikawa, "A study on multirate sampled-data control for hard disk drives," in *Proc. IEE Jpn. Tech. Meeting Industrial Instrumentation and Control*, 2000, IIC-00-55, pp. 31–38.

[9] M. Takiguchi, M. Hirata, and K. Nonami, "Following control of hard disk drives using multi-rate $\mathcal{H}_\infty$ control," in *Proc. SICE Annu. Conf.*, 2002.

[10] T. Semba, "An H_∞ design method for a multi-rate servo controller and applications to a high density hard disk drive," in *Proc. 40th IEEE Conf. Decision and Control*, Dec. 2001, pp. 4693–4698.

[11] K. Ohno, Y. Abe, and T. Maruyama, "Robust following control design for hard disk drives," in *Proc. IEEE Conf. Control Applications*, Sep. 2001, pp. 930–935.

[12] W. Sun, K. M. Nagpal, and P. P. Khargonekar, "$\mathcal{H}_\infty$ control and filtering for sampled-data systems," *IEEE Trans. Autom. Control*, vol. 38, no. 8, pp. 1162–1175, Aug. 1993.

[13] G. F. Franklin, J. D. Powell, and M. Workman, *Digital Control of Dynamic Systems*, 3rd ed. Reading, MA: Addison Wesley, 1998, pp. 649–666.

[14] P. D. Welch, "The use of fast fourier transform for the estimation of power spectra: A method based on time averaging over short, modified periodograms," *IEEE Trans. Audio Electroacoust.*, vol. AU-15, no. 2, pp. 70–73, Jun. 1967.

[15] A. Feuer and G. C. Goodwin, "Generalized sampled hold functions-frequency domain analysis of robustness, sensitivity, and intersample difficulties," *IEEE Trans. Autom. Control*, vol. 39, no. 5, pp. 1042–1047, May 1994.

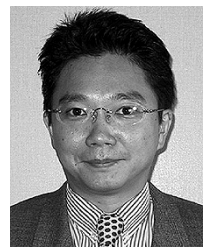

Keitaro Ohno (M'03) was born in Tokyo, Japan, in 1968. He received the B.S. and M.S. degrees in mechanical engineering from the Tokyo Institute of Technology in 1991 and 1993, respectively.

In 1993, he joined the Space Development Group, Fujitsu Laboratories, Ltd., Kanagawa, Japan. Since 1999, he has been with the Autonomous System Laboratory, Fujitsu Laboratories, Ltd., working on the robust head-positioning control of HDDs. From 2001 to 2003, he was a Visiting Industrial Fellow at the Computer Mechanics Laboratory, University of California, Berkeley. His research interests include robust and optimal control in robotics and HDD servo.

Mr. Ohno is a Member of SICE and ASME.

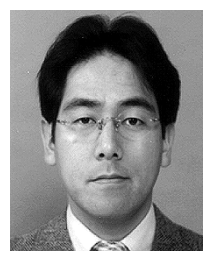

Mitsuo Hirata (M'02) was born in Tokyo, Japan, in 1969. He received the B.E., M.E., and Ph.D. degrees from Chiba University, Chiba, Japan, in 1991, 1993, and 1996, respectively.

From 1996 to 2004, he was a Research Associate with Department of Electronics and Mechanical Engineering, Chiba University. Since June 2004, he has been with the Department of Electrical and Electronic Engineering, Utsunomiya University, Tochigi, where he is currently an Associate Professor. From 2002 to 2003, he was a Visiting Scholar with the Department of Mechanical Engineering, University of California, Berkeley. His research and educational interests include robust control, sampled-data control system design, and motion and vibration control and their applications to various industrial systems, including advanced control of HDDs.

Dr. Hirata is a Member of the Society of Instrument and Control Engineers, Japan, and the Institute of Electrical Engineers of Japan.

Roberto Horowitz (M'89) was born in Caracas, Venezuela, in 1955. He received the B.S. degree (with highest honors) and Ph.D. degree in mechanical engineering from the University of California (UC), Berkeley, in 1978 and 1983, respectively.

In 1982, he joined the Department of Mechanical Engineering, UC, Berkeley, where he is currently a Professor. He teaches and conducts research in the areas of adaptive, learning, nonlinear, and optimal control, with applications to MEMS, computer disk file systems, robotics, mechatronics and IVHS.

Dr. Horowitz is a Member of ASME.